Ultra-High-Sensitivity Submillimeter Mouse SPECT

Oleksandra Ivashchenko[1–3], Frans van der Have[1–3], Marlies C. Goorden[1], Ruud M. Ramakers[1–3], and Freek J. Beekman[1–3]

[1]Section of Radiation, Detection, and Medical Imaging, Delft University of Technology, Delft, The Netherlands; [2]MILabs B.V., Utrecht, The Netherlands; and [3]Department of Translational Neuroscience, Brain Center Rudolf Magnus, University Medical Center Utrecht, Utrecht, The Netherlands

SPECT with submegabecquerel amounts of tracer or subsecond time resolution would enable a wide range of new imaging protocols such as screening tracers with initially low yield or labeling efficiency, imaging low receptor densities, or even performing SPECT outside regular radiation laboratories. To this end we developed dedicated ultra-high-sensitivity pinhole SPECT. **Methods:** A cylindric collimator with 54 focused 2.0-mm-diameter conical pinholes was manufactured and mounted in a stationary small-animal SPECT system. The system matrix for image reconstruction was calculated via a hybrid method based on both ^{99m}Tc point source measurements and ray-tracing analytic modeling. SPECT images were reconstructed using pixel-based ordered-subsets expectation maximization. Performance was evaluated with phantoms and low-dose bone, dynamic kidney, and cardiac mouse scans. **Results:** The peak sensitivity reached 1.3% (13,080 cps/MBq). The reconstructed spatial resolution (rod visibility in a micro-Jaszczak phantom) was 0.85 mm. Even with only a quarter megabecquerel of activity, 30-min bone SPECT scans provided surprisingly high levels of detail. Dynamic dual-isotope kidney and ^{99m}Tc-sestamibi cardiac scans were acquired with a time-frame resolution down to 1 s. **Conclusion:** The high sensitivity achieved increases the range of mouse SPECT applications by enabling in vivo imaging with less than a megabecquerel of tracer activity or down to 1-s frame dynamics.

Key Words: SPECT; pinhole; molecular imaging; low-dose; dynamic imaging

J Nucl Med 2015; 56:470–475
DOI: 10.2967/jnumed.114.147140

The trade-off between resolution and sensitivity is a constant challenge in preclinical SPECT imaging. The small size of the animals that are imaged with preclinical scanners has tended to put the main focus of SPECT development in the last decade on resolution improvements (*1–5*). As a result, the sensitivity (fraction of emitted photons detected) of modern dedicated high-sensitivity multipinhole collimator systems rarely exceeds 0.2%. Improvement of the sensitivity characteristics would offer several significant advantages. Imaging could, for instance, be performed more rapidly, thereby allowing a higher throughput for tracer screening applications or observation of dynamic processes with good time resolution. In addition, with less radioactive tracer needing to be used, it would be possible to, for example, perform in vivo imaging of low-capacity receptor systems, thus aiding research into new tracer compounds or reducing the costs and easing the license requirements of an experiment (Table 1).

Noncollimated high-sensitivity SPECT was developed by Mitchell and Cherry (*6*) using 2 closely spaced scintillator detectors. This approach allows a high (40%) detection efficiency to be reached but currently restricts applications to resolutions at a level of about 1 cm.

The aim of the present work was to develop an ultra-high-sensitivity SPECT system using a collimator that aims to have a high sensitivity and still allow submillimeter-resolution 3-dimensional (3D) and 4-dimensional SPECT imaging. We evaluated the performance of the new collimator using phantoms as well as static and rapid dynamic ultra-low-dose imaging in live mice.

MATERIALS AND METHODS

SPECT System

The new collimator was mounted in the U-SPECT$^+$ (MILabs) series of scanners (*7*). This system uses three 595 × 472 mm NaI (Tl) stationary detectors, a set of replaceable focusing multipinhole collimators, and a user interface that aids both total-body SPECT and 3D focused imaging (*8*). Other details on the original system design have been previously published (*4*).

Collimator Design

The ultra-high-sensitivity collimator is designed to fit mouse-sized animals. It consists of a lead cylinder with an inner bore diameter of 46 mm and a wall thickness of 30 mm (Fig. 1) with fifty-four 2.0-mm-diameter conical pinholes positioned in 4 rings. As one can see from Figure 1, the center of each pinhole is on the inner wall surface of the collimator tube. By not having a conical part of the pinhole on the inside, we intended to minimize the object–pinhole distance and maximize the pinhole–detector distance, in order to additionally improve sensitivity and resolution (by increasing magnification factor) characteristics. The 2 most central rings (2 and 3; Fig. 1) contain 15 pinholes with 25.1° opening angles, whereas the outer rings (1 and 4; Fig. 1) contain a combination of 12 pinholes with a 21.2° or 24.2° opening angle. All pinholes together form an hourglass-shaped field of view (FOV; Fig. 1) that is used for data acquisition via a scanning focus method (*9*). The central part of the FOV (an ellipsoid of 12 × 12 × 7 mm), or the so-called central FOV (Fig. 1), is seen by all pinholes simultaneously and provides complete data without any bed movement (i.e., within a single bed position). Images from each pinhole are directly projected on the surface of the detector and create slightly overlapping projections.

System Calibration and Image Reconstruction

The exact geometry of the system was determined by ^{99m}Tc point source measurements (*10*), and the system matrix was subsequently calculated by an analytic model based on ray tracing (*11*).

Received Sep. 3, 2014; revision accepted Jan. 5, 2015.
For correspondence or reprints contact: Oleksandra Ivashchenko, Reactor Institute Delft, Section of Radiation, Detection, and Medical Imaging, Mekelweg 15, 2629 JB, Delft, The Netherlands.
E-mail: o.ivashchenko-1@tudelft.nl
Published online Feb. 12, 2015.

TABLE 1
Example Exemption Limits for Several SPECT Isotopes

Radionuclide	Activity (MBq)	
	The Netherlands*	United States†
^{99m}Tc	10	37
^{111}In	1	3.7
^{123}I	10	3.7
^{67}Ga	1	37

*National Radiological Protection Board of Kingdom of Netherlands (NRPB-R306), directive 96/29.

†U.S. Nuclear Regulation Commission, title 10 of *Code of Federal Regulations* appendix C to part 20.

If amount of activity that is used in total is kept below these limits, license to perform experiment is not required.

Images were reconstructed from the list-mode data using pixel-based ordered-subsets expectation maximization (*12*) with resolution recovery and compensation for distance-dependent pinhole sensitivity. For all SPECT images shown, we used 32 subsets, 15 iterations, and an isotropic 0.4-mm-voxel grid. Compton scatter correction was applied via the triple-energy-window method (*13*) with use of either one 20% (centered at 140 keV) or two 15% (centered at 171 and 245 keV) photopeak windows for ^{99m}Tc and ^{111}In isotopes, respectively. The background windows were placed on each side of the photopeak with a width of 3% (^{99m}Tc) and 2.5% (^{111}In) of the corresponding photopeak. All images were attenuation-corrected as described by Wu et al. (*14,15*). The reconstructed volumes of all SPECT scans were postfiltered with a 3D gaussian filter of 1.0 mm in full width at half maximum. Time–activity curves were generated for manually drawn volumes of interest (VOIs), using decay-corrected but otherwise unprocessed images, reconstructed as a dynamic frame sequence.

Phantom Scans

The sensitivity of the collimator along the axial and transaxial directions was measured in counts per second per megabecquerel of activity (cps/MBq) by scanning a ^{99m}Tc point source of known activity (*4,10*) through the center of the FOV. The resolution was determined with micro-Jaszczak hot-rod capillary resolution phantom scans. The phantom consisted of 6 sections with rods 1.7, 1.5, 1.3, 1.0, 0.95, and 0.85 mm in diameter, which together provided a 0.21-mL volume for filling with activity. The minimum distance between the capillaries in each section equalled the capillary diameter in that section. The phantom was filled with 0.25 or 5 MBq of ^{99m}Tc-pertechnetate (concentrations of 1.19 and 23.8 MBq/mL, respectively). Dynamic 30-min acquisitions using 5-min frames were performed.

Animal Studies

The animal experiments were performed with C57BL/6 mice according to protocols approved by the Animal Ethics Committee of the UMC Utrecht and in accordance with Dutch Law on Animal Experimentation. All SPECT scans were acquired for 30 min with the ultra-high-sensitivity collimator. Every animal used for imaging was anesthetized with isoflurane and injected with tracer activity via the tail vein. For dynamic image acquisitions, a tail vein catheter was used for the tracer injections.

Low-Dose Bone SPECT Scans

Two mice were anesthetized and injected with 0.25 or 3.5 MBq of ^{99m}Tc-methylene diphosphonate respectively. Half an hour after the injection, subsequent total-body, focused pelvis, and focused skull scans were performed for each animal. The total number of bed positions used during data acquisition in those scans varied from 7 (focused skull) to 45 (total body), dependent on the animal and corresponding scan area sizes.

Microdose Renal Function SPECT

A mouse was anesthetized, and the kidneys were selected as the scan area of interest, which required 2 bed positions. Just after the start of the dynamic SPECT acquisitions with 15-s frames, the mouse was injected with 1.5 MBq of ^{99m}Tc-mercaptoacetyltriglycine (MAG3) and 1.5 MBq of ^{111}In-diethylene triamine pentaacetic acid (DTPA). The time between the 2 activity injections was around 45 s. Time–activity curves were generated for 2 VOIs, which were manually drawn around each kidney. The curves were smoothed via use of nearest-neighbor averaging over 3 points.

Fast Dynamic Cardiac Scan

Two mice were anesthetized, and the heart was selected as the scan area of interest, which required only 1 bed position. Just after the start of the dynamic SPECT acquisitions with 1-s frames, the mice were injected with either 9 MBq (mouse 1) or 15 MBq (mouse 2) of ^{99m}Tc-sestamibi. Time–activity curves were generated for equally sized spheric VOIs placed in the aorta and myocardial tissue regions. The required size and position of the VOIs

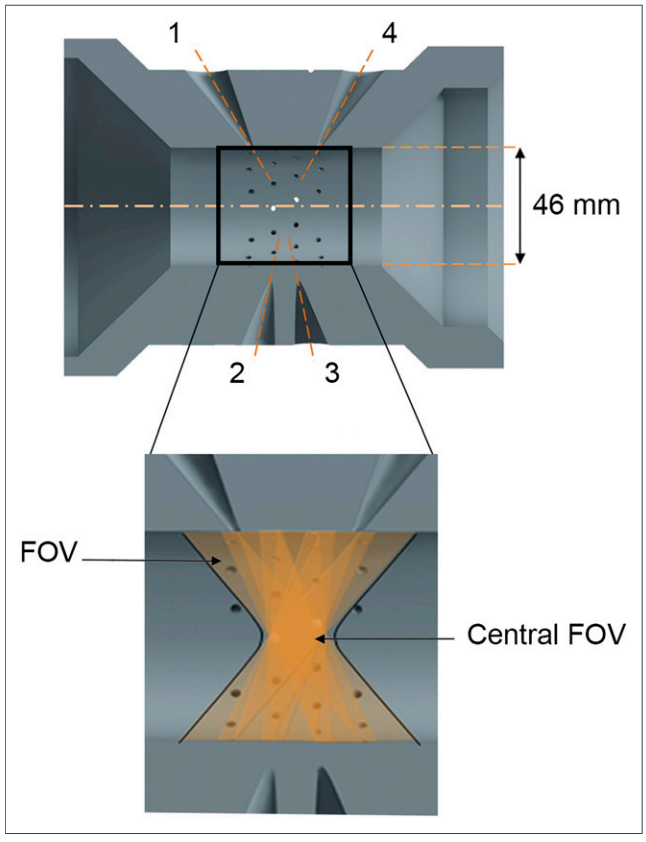

FIGURE 1. Cross-section of ultra-high-sensitivity collimator with illustration of pinholes positioned in 2 outer (1 and 4) and 2 inner (2 and 3) pinhole rings. Zoomed view (bottom) on central part of collimator illustrates shape and position of FOV (orange area).

were determined from the reconstructed volume for the total duration of the scan. The time–activity curves were subsequently generated from the dynamic image sequence (for minutes 0–10 of the acquisition) and smoothed via nearest-neighbor averaging over 3 points.

RESULTS

Phantom Studies

Figure 2A shows 4-mm-thick slices (sum of 10 subsequent 0.4-mm-thick slices) from the dynamic micro-Jaszczak resolution phantom scans with ^{99m}Tc. Even for the shortest acquisition of 5 min, rods with diameters down to 1.1 mm using 0.25 MBq and down to 0.85 mm using 5 MBq could be distinguished. Within 30 min of acquisition, the minimal visible rod diameter for the 0.25-MBq scan improved to 0.95 mm. Figure 2B illustrates sensitivity profiles along the axial (z) and transaxial (x) directions through the center of the FOV. The peak sensitivity for ^{99m}Tc at the center of the collimator was determined to be 1.3% (13,080 cps/MBq) and decreased to the lowest values of 1.0% (along z) and 0.81% (along x) at the edges of the central FOV.

Low-Dose Bone Scans

Figure 3 shows maximum-intensity projections of the ^{99m}Tc-methylene diphosphonate mouse total-body, focused pelvis, and focused skull scans. The top- and side-view maximum-intensity projections of the total-body scan illustrated that a 3.5-MBq scan provided details of the anatomic structures in the mouse skeleton, such as in the pelvis, skull, and both upper and lower limbs. A decrease in the injected tracer activity by a factor of 14 (down to 0.25 MBq) degraded the visible level of detail, but the resulting image still revealed the 3D anatomic structure of the skeleton.

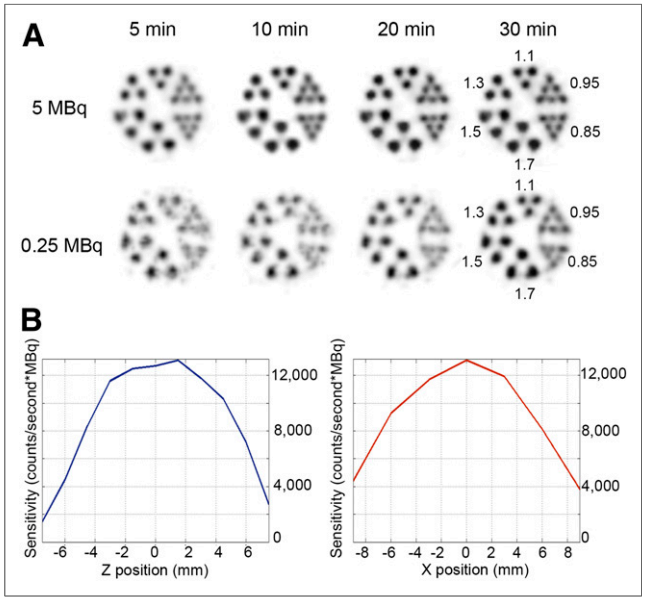

FIGURE 2. (A) ^{99m}Tc resolution phantom scans (5 and 0.25 MBq) for different acquisition times (5, 10, 20, and 30 min). Smallest visible rod diameter for 30-min acquisition was 0.85 mm. In 5-min acquisitions, 1.1-mm rods can be seen for all activities used. (B) Sensitivity profiles for single bed position along axial (z) and transaxial (x) directions through center of collimator's FOV for ^{99m}Tc.

Reconstructions of separate focused pelvis and skull scans show improvement of images in terms of visible details compared with the total-body images obtained with the same tracer activity.

Dual-Isotope Kidney Scan

Figure 4 presents the ^{99m}Tc-MAG3/^{111}In-DTPA dynamic kidney scan. Both tracers are primarily used for evaluation of tubular filtration and result in rapid renal clearance of the compound (*16,17*). Fast clearance of the tracers in combination with animal size–related limitations for maximally allowed volumes of injections (0.2 mL/animal for the intravenous administration routes) (*18*) and low labeling efficiency of ^{111}In-DTPA (*19*) hampers application of those tracers for SPECT imaging with mice, particularly when dynamic imaging needs to be performed. Figure 4A shows a set of individual 15-s frames (slice thickness, 2 mm) that illustrates the difference in the tracers' dynamics. It was clear that renal filtration of ^{111}In-DTPA took place mainly in the medulla cavity region, whereas filtration of ^{99m}Tc-MAG3 involved both the renal cortex and the medulla cavity. Also, ^{99m}Tc-MAG3 followed 3 defined stages of filtration: uptake (0–75 s), plateau (75–180 s), and clearance (180–1,800 s). In the case of ^{111}In-DTPA, uptake of the compound (0–120 s) was rapidly followed by the clearance stage (120–1,800 s), with no noticeable plateau. Such results agree with both the individual biodynamics of the tracers (*20,21*) and the simultaneous dynamics of the tracers as shown on the time–activity curves (Fig. 4B), indicating that the tracers reach maximal uptake around 130 s after injection and are washed out within 600 s. The relatively short delay in the beginning of ^{111}In-DTPA uptake on the time–activity curves can be explained by the 45-s difference between the injection times of the 2 tracers that was not considered during time–activity curve generation or during division onto tracer uptake stages.

Fast Dynamic Cardiac Scan

Figure 5 shows 0.4-mm-thick slices from the short (Fig. 5A) and long (Fig. 5B) cardiac axes, obtained from reconstructions of a 10-min acquisition segment (minutes 4–14) of the dynamic 30-min ^{99m}Tc-sestamibi scan (mouse 1). The images illustrate a clear separation between the left and right ventricular walls, as well as details of the myocardium. The time–activity curve of the tracer dynamic in the aorta (Fig. 5C) contains 2 defined peaks of tracer concentration around the 30- and 70-s time points. Most probably, the first peak corresponds to the initial pass of activity through the heart. The presence of the second peak at the 70-s time point can be explained by the secondary activity infusion in the animal during the postinjection flushing of the tail vein catheter with saline. We assume that the difference in amplitude and peak position on time–activity curves shown in Figure 5C was caused by differences in activity injection speeds between those 2 experiments. The tracer concentration in the myocardial tissue rapidly increased after each activity infusion and retained a constant level for the remaining time of the scan.

DISCUSSION

The size of the animals that are used in preclinical molecular imaging sets 2 main requirements for the performance characteristics of preclinical SPECT scanners. Their resolution needs to be high enough to allow visualization of sufficient detail, and their sensitivity needs to be high enough to produce a sufficient counting rate even with only small amounts of injected activity. The current work showed the results of the evaluation of a new ultra-high-sensitivity collimator

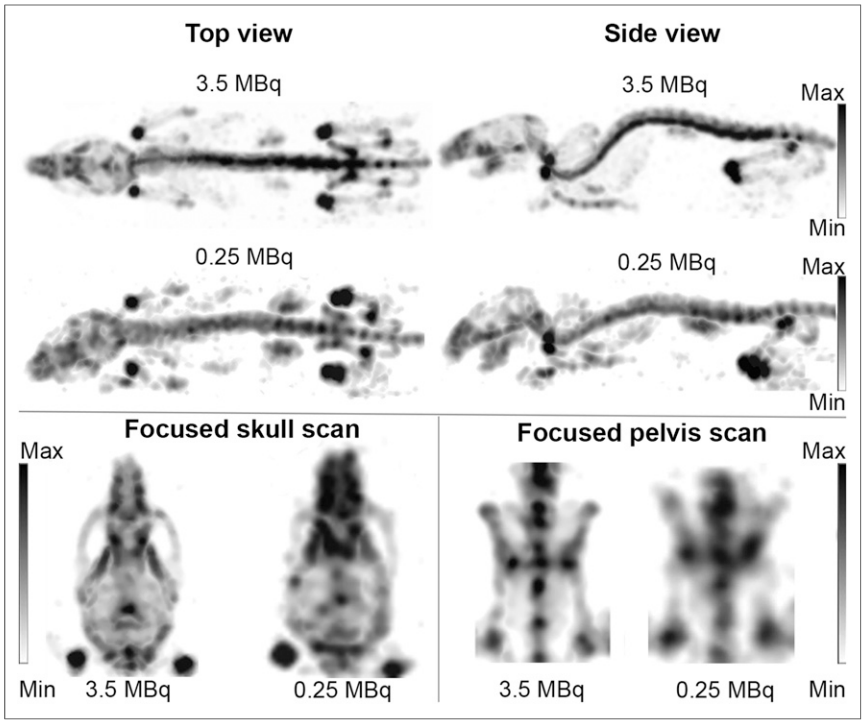

FIGURE 3. Top and side maximum-intensity projections of 30-min total-body ^{99m}Tc-methylene diphosphonate mouse scan. In 3.5-MBq scan, high level of anatomic detail is provided in upper and lower limbs, pelvis, and skull. In 0.25-MBq scan, uptake in entire skeleton can be detected, and skull and pelvis still show high level of detail. When focused scans were performed, image quality was obviously improved for both scan areas (skull and pelvis) and levels of tracer activity.

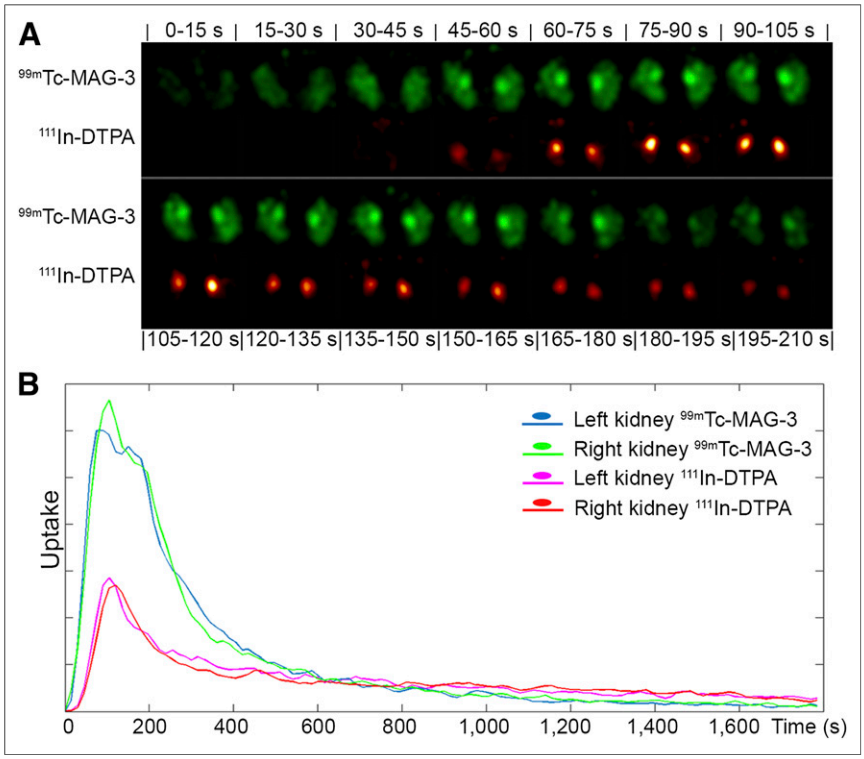

FIGURE 4. (A) 2-mm-thick slices of dynamic 15-s frames for dual-isotope ^{99m}Tc-MAG3 (green) and ^{111}In-DTPA (orange) kidney scan (time delay between injections was 45 s). Images illustrate difference in tracer dynamics, with slower uptake/clearance and longer plateau for ^{99m}Tc-MAG3 than for ^{111}In-DTPA. (B) Time–activity curves of ^{111}In-DTPA/^{99m}Tc-MAG3 uptake by left and right kidneys.

that allows 3D submillimeter mouse SPECT and ultra-low-dose or fast dynamic imaging applications in the U-SPECT$^+$ system.

The resolution phantom scans illustrated that the collimator can reach its peak 0.85-mm reconstructed image resolution within a 5-min acquisition with 5 MBq in a Jaszczak phantom and can even maintain a submillimeter resolution (0.95 mm) with 0.25 MBq when a longer acquisition (30 min) is used. The peak sensitivity of the collimator reached 1.3% for ^{99m}Tc, which slightly exceeds an estimated value of 1.2% for the double-cone pinhole geometry model (*22*). Such performance makes the collimator most suitable for either submegabecquerel static scans or several-megabecquerel fast dynamic scans.

The results of the animal evaluation on low-dose bone imaging illustrated that quite a high level of detail can be achieved with just several megabecquerels (3.5 MBq) or even 0.25 MBq when static images are acquired. When finer details are needed for the same activity level, local focusing on the area of interest (Fig. 3, skull and pelvis) can be used to improve resolution and general image quality. This application of focused scanning (*8,9*) can benefit imaging with tracers that cannot reach high labeling efficiency or imaging of organs and tissues with relatively low specific uptake (e.g., different tumors or the brain).

Often, to obtain good time resolution, dynamic SPECT imaging requires injection of high tracer activities. Because of size-related limitations on maximally allowed injection volumes (*18*), dynamic imaging in mice either requires the use of tracers with high activity concentrations or results in long time frames (*23*). The kidney scan shown in this work demonstrates that with the ultra-high-sensitivity collimator, a time frame of as low as 15 s can be reached with a submegabecquerel level of activity. This ability allows analysis of tracer dynamics not just from the time–activity curves but also from the dynamic sequence of SPECT images, illustrating the biodistribution of the radiolabeled compound within the organ or system of organs. At the same time, if scans need to be repeated, the low level of required activity would prevent a harmful radiation dose from accumulating in the animal or influencing the reliability of the results. The frame rate of SPECT can be further increased by the use of higher tracer activities

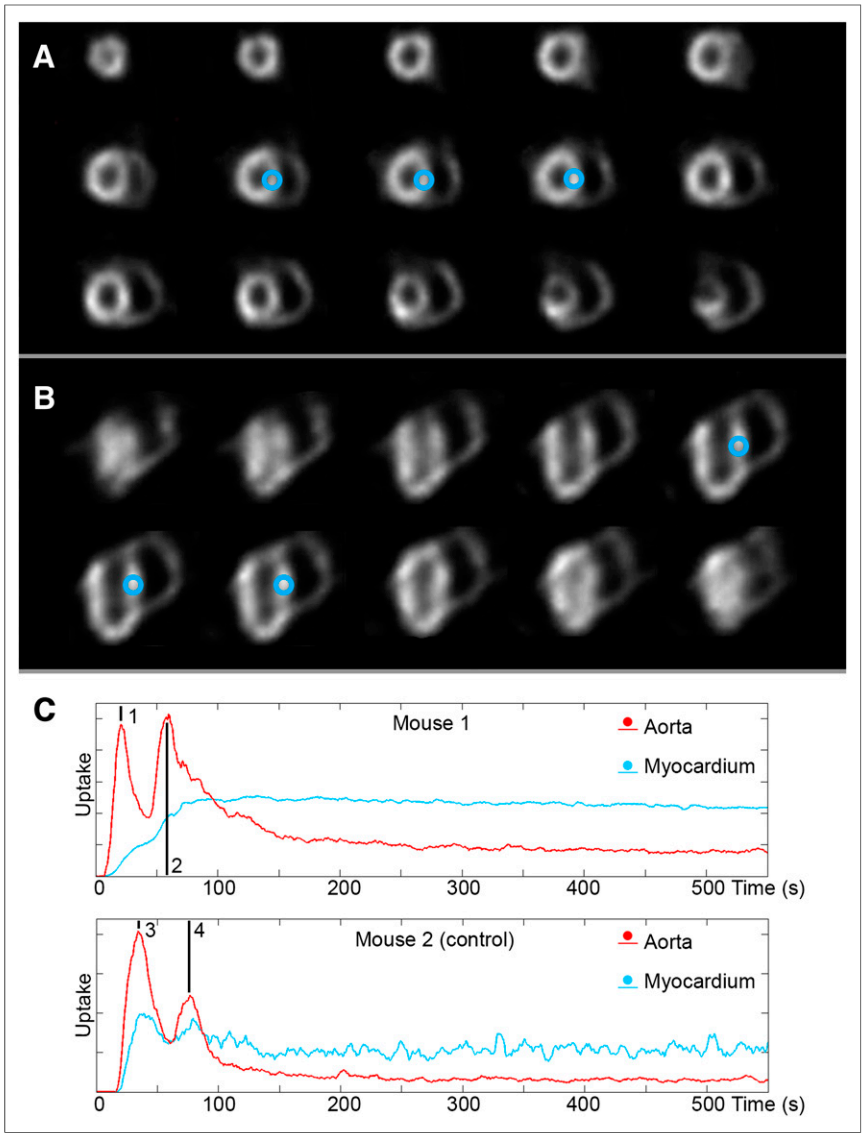

FIGURE 5. (A and B) 0.4-mm-thick slices of short and long axes through mouse heart (mouse 1), obtained from reconstructions of 10-min segment of 30-min focused ^{99m}Tc-sestamibi scan. These images clearly show separation between left and right ventricular walls, as well as details of myocardial structure. (C) Time–activity curves visualize 1-s time resolution tracer dynamics in aorta and myocardial tissue. Arrows 1 and 2 (mouse 1) and 3 and 4 (mouse 2) indicate first pass of activity in aorta after initial activity injection and secondary activity infusion of ^{99m}Tc-sestamibi, respectively. VOI used for generation of myocardial tissue time–activity curves is indicated with circles in A and B.

or more focused scanning applying a small number of bed positions. Scanning of the area that occupies several bed positions will require overhead time for animal bed movement that ultimately will present the main limitation on the shortest possible frame length for SPECT acquisitions. When the organ or scan area of interest fits within the central FOV (as in the case of the cardiac scan presented in Fig. 5), time frames can be shortened to 1 s. However, because of the high sensitivity of this collimator, focused scanning with more than approximately 30 MBq in the central FOV (using the U-SPECT$^+$ system) will result in more than a 20% count loss, partly because of the limitations of currently used read-out electronics.

CONCLUSION

The current work has evaluated an ultra-high-sensitivity mouse SPECT collimator that has 1.3% peak sensitivity and still reaches a 0.85-mm reconstructed spatial resolution for ^{99m}Tc. The animal scans presented in this paper illustrate the possibility of performing dynamic SPECT with 1-s time frames or performing static SPECT with tiny amounts of activity (fractions of a megabecquerel). On the basis of its performance, the collimator can be used in several ways: to reduce the animal dose during follow-up molecular imaging studies; to improve the frame rate for dynamic biokinetic screening during the development of new tracers or imaging of biologic processes with fast dynamics; to increase the possible number of applications for imaging of organs that have low specific uptake or for tracers and nanocarriers that have low labeling efficiency; to reduce the cost of a study; or even to simplify the radiation safety license application procedure via reduction of required activities (in some cases below the radiation safety license exemption level, Table 1).

DISCLOSURE

The costs of publication of this article were defrayed in part by the payment of page charges. Therefore, and solely to indicate this fact, this article is hereby marked "advertisement" in accordance with 18 USC section 1734. The research leading to these results received funding from the People Programme (Marie Curie Actions) of the European Union's Seventh Framework Programme (FP7/2007-2013) under REA grant agreement PITN-GA-2012-317019 TRACE 'n TREAT. Freek J. Beekman is a founder, shareholder, and part-time board member of MILabs. Frans van der Have is a shareholder of MILabs. No other potential conflict of interest relevant to this article was reported.

REFERENCES

1. Schramm NU, Ebel G, Engeland U, Schurrat T, Béhé M, Behr TM. High-resolution SPECT using multi-pinhole collimation. *IEEE Trans Nucl Sci.* 2003;50:315–320.
2. Beekman FJ, Have F, Vastenhouw B, et al. U-SPECT-I: a novel system for submillimeter-resolution tomography with radiolabeled molecules in mice. *J Nucl Med.* 2005;46:1194–1200.
3. Nuyts J, Vunckx K, Defrise M, Vanhove C. Small animal imaging with multi-pinhole SPECT. *Methods.* 2009;48:83–91.
4. van der Have F, Vastenhouw B, Ramakers RM, et al. U-SPECT-II: an ultra-high-resolution device for molecular small-animal imaging. *J Nucl Med.* 2009;50:599–605.
5. Deleye S, Van Holen R, Verhaeghe J, Vandenberghe S, Stroobants S, Staelens S. Performance evaluation of small-animal multipinhole μSPECT scanners for mouse imaging. *Eur J Nucl Med Mol Imaging.* 2013;40:744–758.

6. Mitchell GS, Cherry SR. A high-sensitivity small animal SPECT system. *Phys Med Biol.* 2009;54:1291–1305.
7. Ivashchenko O, van der Have F, Villena JL, et al. Quarter-millimeter-resolution molecular mouse imaging with U-SPECT^{+}. *Mol Imaging.* 2014;13:1–8.
8. Branderhorst W, Vastenhouw B, van der Have F, Blezer ELA, Bleeker WK, Beekman FJ. Targeted multi-pinhole SPECT. *Eur J Nucl Med Mol Imaging.* 2011;38:552–561.
9. Vastenhouw B, Beekman FJ. Submillimeter total-body murine imaging with U-SPECT-I. *J Nucl Med.* 2007;48:487–493.
10. van der Have F, Vastenhouw B, Rentmeester M, Beekman FJ. System calibration and statistical image reconstruction for ultra-high resolution stationary pinhole SPECT. *IEEE Trans Med Imaging.* 2008;27:960–971.
11. Goorden MC, van der Have F, Kreuger R, Beekman FJ. An efficient simulator for pinhole imaging of PET isotopes. *Phys Med Biol.* 2011;56:1617–1634.
12. Branderhorst W, Vastenhouw B, Beekman FJ. Pixel-based subsets for rapid multi-pinhole SPECT reconstruction. *Phys Med Biol.* 2010;55:2023–2034.
13. Ogawa K, Harata Y, Ichihara T, Kubo A, Hashimoto S. A practical method for positron-dependent Compton-scatter correction in single photon emission CT. *IEEE Trans Med Imaging.* 1991;10:408–412.
14. Wu C, Gratama van Andel HA, Laverman P, Boerman OC, Beekman FJ. Effects of attenuation map accuracy on attenuation-corrected micro-SPECT images. *EJNMMI Res.* 2013;3:7.
15. Wu C, de Jong JR, Gratama van Andel HA, et al. Quantitative multi-pinhole small-animal SPECT: uniform versus non-uniform Chang attenuation correction. *Phys Med Biol.* 2011;56:N183–N193.
16. Melis M, de Swart J, de Visser M, et al. Dynamic and static small-animal SPECT in rats for monitoring renal function after ^{177}Lu-labeled Tyr^{3}-octreotite radionuclide therapy. *J Nucl Med.* 2010;51:1962–1968.
17. Sfakianakis GN, Georgiou MF. MAG3 SPECT: a rapid procedure to evaluate the renal parenchyma. *J Nucl Med.* 1997;38:478–483.
18. Van Zutphen LFM, Baumans V, Beynen AC. *Principles of Laboratory Animal Science*. Revised ed. Amsterdam, The Netherlands: Elsevier; 2001: 317.
19. Brom M, Joosten L, Oyen WJ, Gotthardt M, Boerman OC. Improved labelling of DTPA- and DOTA-conjugated peptides and antibodies with ^{111}In in HEPES and MES buffer. *EJNMMI Res.* 2012;2:4.
20. Jouret F, Walrand S, Parreira KS, et al. Single photon emission-computer tomography (SPECT) for functional investigation of the proximal tubule in conscious mice. *Am J Physiol Renal Physiol.* 2010;298:F454–F460.
21. Tantawy MN, Jiang R, Wang F, et al. Assessment of renal function in mice with unilateral ureteral obstruction using ^{99m}Tc-MAG3 dynamic scintigraphy. *BMC Nephrol.* 2012;13:168.
22. Rentmeester MC, van der Have F, Beekman FJ. Optimizing multi-pinhole SPECT geometries using an analytical model. *Phys Med Biol.* 2007;52:2567–2581.
23. Vaissier PE, Goorden MC, Vastenhouw B, van der Have F, Ramakers RM, Beekman FJ. Fast spiral SPECT with stationary γ-cameras and focusing pinholes. *J Nucl Med.* 2012;53:1292–1299.